

## High-Efficiency Isolated Bidirectional Ac Dc Converter For A Dc Distribution System

B.Krishnakanth <sup>1</sup>, P.Siva Krishna <sup>2</sup> M.Tech

Brahmaiah College Of Engineering  
Electrical and Electronics Engineering  
North Rajupalem,kovur-524137  
Email: krishnakanth.eee09@gmail.com

**Abstract**—A high-efficiency isolated bidirectional ac–dc converter is proposed for a 380-V dc power distribution system to control bidirectional power flows and to improve its power conversion efficiency. To reduce the switches' losses of the proposed nonisolated full-bridge ac–dc rectifier using an unipolar switching method, switching devices employ insulated-gate bipolar transistors, MOSFETs, and silicon carbide diodes. Using the analysis of the rectifier's operating modes, each switching device can be selected by considering switch stresses. A simple and intuitive frequency detection method for a single-phase synchronous reference frame-phase-locked loop (SRF-PLL) is also proposed using a filter compensator, a fast period detector, and a finite impulse response filter to improve the robustness and accuracy of PLL performance under fundamental frequency variations. In addition, design and control methodology of the bidirectional full-bridge *CLLC* resonant converter is suggested for the galvanic isolation of the dc distribution system. A dead-band control algorithm for the bidirectional dc–dc converter is developed to smoothly change power conversion directions only using output voltage information. Experimental results will verify the performance of the proposed methods using a 5-kW prototype converter

**Index Terms**—AC–DC boost rectifier, bidirectional isolated converter, *CLLC* resonant converter dc distribution system.

### I. INTRODUCTION

DC DISTRIBUTION system is one of important future power systems to save energy and to reduce CO<sub>2</sub> emission because it can improve the efficiency of systems due to the reduction of the number of power conversion stages [1]–[3]. Especially, the dc distribution system for a residential house using dc home appliances can allow the flexibility of merging many renewable energy sources because most of the output of renewable energy sources is dc. The overall system configuration of the proposed 380-V dc distribution system is shown in Fig. 1. In order to balance the power flow and to regulate the dc-bus voltage, the dc distribution system requires an isolated bidirectional ac–dc converter to interface between dc bus and ac grid. It usually consists of a nonisolated bidirectional ac–dc rectifier [4]–[9] for grid-connected operation and an isolated bidirectional dc–dc converter to interface dc bus and dc link of the rectifier [10]–[18]

bipolar and the unipolar switching modes. One of the disadvantages of the bipolar switching mode is the need of a large

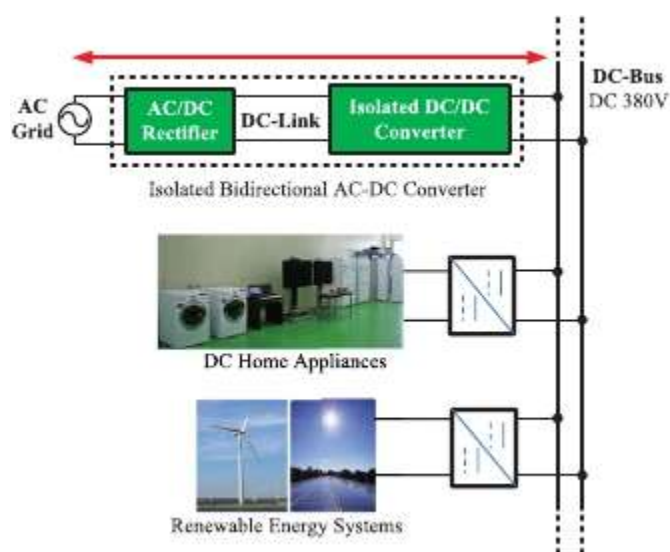


Fig. 1. 380-V dc distribution system with an isolated bidirectional ac–dc converter.

inductor to reduce the input current ripple because the peak-to-peak voltage of the inductor is more than twice the unipolar switching mode. If the full-bridge rectifier operates in the unipolar switching mode, inductance for a continuous current mode (CCM) power factor correction (PFC) operation can be reduced. One of full-bridge rectifier legs in the unipolar switching mode is operated at a line frequency while the other one is modulated at a switching frequency. However, the unipolar switching mode rectifier using conventional switching devices including a normal antiparallel diode causes high reverse recovery current and turn-on switching noise. The switching and the conduction losses in the bidirectional rectifier are the main cause of decreasing power conversion efficiency.

The phase estimation, so-called phase-locked loop (PLL), is required to control the bidirectional ac–dc rectifier; especially, the phase information of supply voltage is mandatory to generate a current reference. One of the popular PLL methods is synchronous reference frame (SRF-PLL) which uses

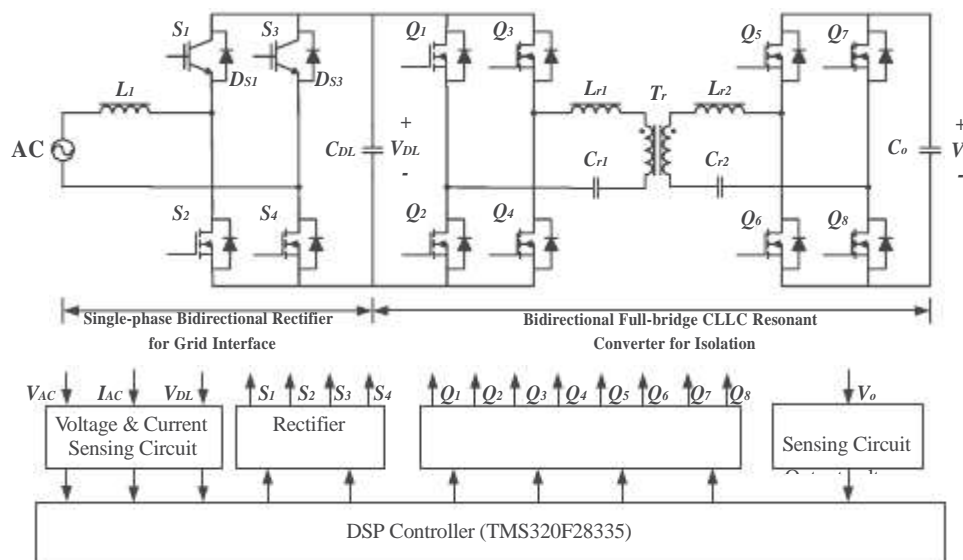


Fig. 2. Circuit configuration of the proposed isolated bidirectional ac-dc converter.

rotating reference frame for tracking a phase angle. However, the conventional SRF-PLL has a weak point of frequency tracking performance because it uses the constant angular frequency of a fundamental component. It can cause a tracking error in the PLL operation when the fundamental frequency changes to the different value of the constant angular frequency. Numerous methods for improved PLL have been presented and introduced in the literature [19]–[23]. Even though they have good performance against the frequency distortion, their algorithms are complicated to be implemented for various applications. Another PLL method has been proposed using a simple frequency detector and trigonometric calculations without any linear phase detector; however, this method requires the half-cycle data acquisition of the fundamental frequency to detect the exact line frequency [24]. Therefore, a more simple, faster, and more intuitive frequency detection method should be upgraded for improving the performance of the single-phase bidirectional rectifier.

Some isolated full-bridge bidirectional dc-dc converter topologies have been presented in recent years. A boost full-bridge zero-voltage switching (ZVS) PWM dc-dc converter was developed for bidirectional high-power applications. However, it needs extra snubber circuits to suppress the voltage stress of the switches [25]–[28]. A bidirectional phase-shift full-bridge converter was proposed with high-frequency galvanic isolation for energy storage systems [29], [30]. This converter can improve power conversion efficiency using a zero-voltage transition feature; however, it requires input voltage variations to regulate constant output voltage because this topology can only achieve the step-down operation. A bidirectional full-bridge LLC resonant converter was introduced for a UPS system without any snubber circuits [17]. This topology can operate under soft-switching conditions of primary switches and secondary rectifier. In addition, the topology confines voltage stresses without any clamp circuits. However, application of this converter showed different operations between transformer's turn ratio and the difference of resonant networks. Therefore, the novel

design guides suitable for a 380-V dc distribution system should be proposed.

In this paper, the high-efficiency isolated bidirectional ac-dc converter system with several improved techniques will be discussed to improve the performance of a 380-V dc distribution system. In order to increase the efficiency of the nonisolated full-bridge ac-dc rectifier, the switching devices are designed by using insulated-gate bipolar transistors (IGBTs) without an antiparallel diode, MOSFETs, and silicon carbide (SiC) diodes. Through the analysis of operational modes, each switch is selected by considering switch stresses. The major novelty of the proposed PLL is the suggestion of a simple and intuitive frequency detection method for the single-phase SRF-PLL using an advanced filter compensator, a fast quad-cycle detector, and a finite impulse response (FIR) filter. Finally, design guides and gain characteristics of the bidirectional full-bridge CLLC resonant converter with the symmetric structure of the primary inverting stage and secondary rectifying stage will be discussed for a 380-V dc distribution system. Experimental results will verify the performance of the proposed methods using a 5-kW prototype converter.

## II. CIRCUIT CONFIGURATION OF THE PROPOSED ISOLATED BIDIRECTIONAL AC-DC CONVERTER

Fig. 2 shows the circuit configuration of the proposed isolated bidirectional ac-dc converter. It consists of the single-phase bidirectional rectifier for grid interface and the isolated bidirectional full-bridge CLLC resonant converter for galvanic isolation. To control the proposed converter, a single digital signal processor (DSP) controller (TMS320F28335) was used. The power flow directions in the converter are defined as follows: rectification mode (forward direction of power flow) and generation mode (backward direction of power flow).

The switching method of the proposed single-phase bidirectional rectifier is unipolar SPWM. In order to reduce the switching losses caused by the reverse recovery current in the

rectification mode, the high-side switches of the proposed rectifier are composed of two IGBTs without antiparallel diodes ( $S_1$  and  $S_3$ ) and two SiC diodes ( $D_{S1}$  and  $D_{S3}$ ). The low-side switches are composed of two MOSFETs ( $S_2$  and  $S_4$ ) for reducing conduction loss and for using ZVS operation in the generation mode. The detailed circuit operation of the proposed bidirectional rectifier and advanced PLL method will be discussed in Section III.

The proposed bidirectional full-bridge *CLLC* resonant converter has the full-bridge symmetric structure of the primary inverting stage and secondary rectifying stage with a symmetric transformer. Using the high-frequency transformer, the converter can achieve galvanic isolation between the primary side and the secondary side. The transformer  $T_r$  is modeled with the magnetizing inductance  $L_m$  and the transformer's turn ratio of 1:1. The leakage inductance of the transformer's primary and secondary windings is merged to the resonant inductor  $L_{r1}$  and  $L_{r2}$ , respectively. The resonant capacitors  $C_{r1}$  and  $C_{r2}$  make automatic flux balancing and high resonant frequency with  $L_{r1}$  and  $L_{r2}$ . The detailed analysis and design guides of the proposed converter will be discussed in Section IV.

### III. NONISOLATED AC–DC BIDIRECTIONAL RECTIFIER

High-power rectifiers do not have a wide choice of switching devices because there are not many kinds of the switching devices for high-power capacity. Generally, the full-bridge rectifier in high-power applications consists of the same four devices: IGBT modules or intelligent power modules (IPMs) are chiefly used. This modular devices have antiparallel diodes, which have fast recovery characteristics. A fast recovery diode (FRD) has a small reverse recovery time  $t_{rr}$ . When the full-bridge rectifier operates, the time  $t_{rr}$  causes a reverse recovery current which increases power loss and EMC problems. Therefore, soft-switching techniques using additional passive or active snubber circuits have been proposed [31]–[33]. Even though these methods require a relatively large number of passive or active components, which decrease the reliability of the rectifier system and increase system cost, the soft-switching techniques in the high-power rectifier are a unique solution for reducing the reverse recovery problems. On the other hand, a medium-power rectifier system around 5 kW for a residential house or building has a wide selection of switching devices such as discrete-type IGBTs and MOSFETs. Especially, commercial IGBTs without the antiparallel diode can be selected to replace antiparallel FRDs to SiC diodes. In theory, the SiC diode does not have  $t_{rr}$ . Therefore, the combination of IGBTs without the antiparallel diode and the SiC diodes is another viable solution to reduce the reverse recovery problems.

In the bidirectional rectifier using the unipolar switching method, the turn-on period of low-side switches increases one and half times more than the turn-on period of the high-side switches. Therefore, the low-side switches should be chosen to consider low conduction losses for increasing the power conversion efficiency. The latest generation of MOSFETs employing superjunction technology can achieve extremely low on-resistance  $R_{DS(on)}$ . It is better than the latest very low  $V_{CE}$

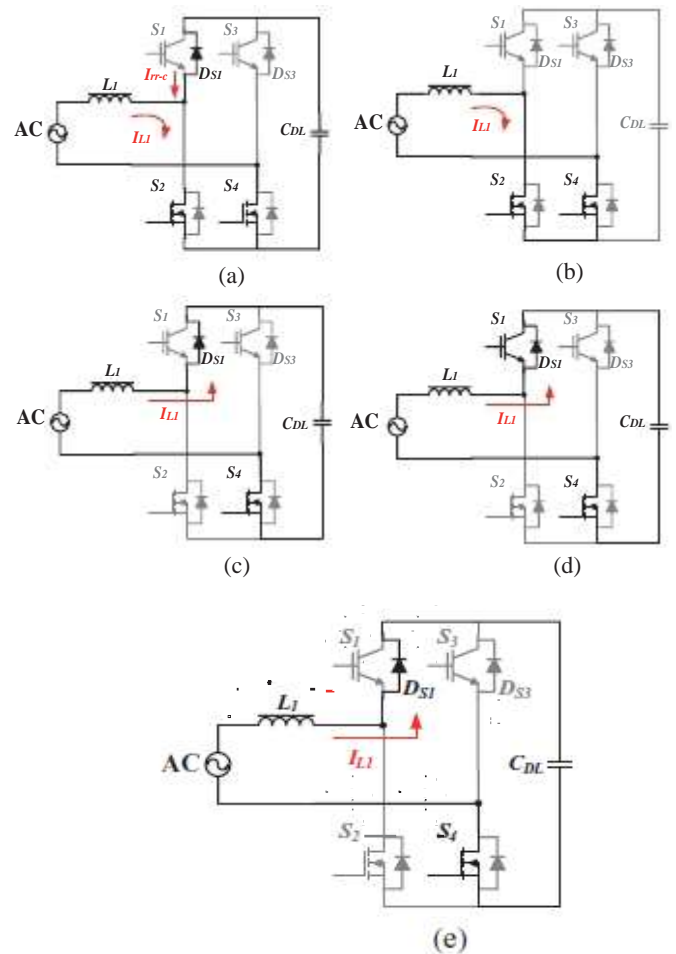


Fig. 3. Operating modes of the proposed bidirectional ac–dc rectifier in the rectification mode: (a) *Mode 1*, (b) *Mode 2*, (c) *Mode 3*, (d) *Mode 4*, and (e) *Mode 5*.

IGBTs in the view point of the conduction loss when the same current flows into the switching devices. Therefore, MOSFETs are suitable for the low-side switches in the unipolar switching method.

#### A. Consideration for Reverse Recovery Losses in a Rectification Mode

In the rectification mode, the bidirectional rectifier has five operating modes in a single switching cycle. The circuit operations in the positive half period of the input voltage are shown in Fig. 3. The dark lines denote conducting paths for each state. The theoretical waveforms of the proposed rectifier are given in Fig. 4.

At time  $t_0$ , the low-side switch  $S_2$  turns ON. At this time, if  $D_{S1}$  is FRD,  $D_{S1}$  cannot immediately turn OFF because of its reverse recovery process. This simultaneous high reverse recovery current causes an additional switching loss on  $S_2$ . The reverse recovery current increases the current stress on the low-side switches and decreases the EMI performance of the rectifier. To solve this reverse recovery problem, the high-side switches of the proposed circuit should use IGBTs without antiparallel diodes and SiC diodes as antiparallel diodes of the IGBTs. Even though the reverse recovery current is not completely zero in a



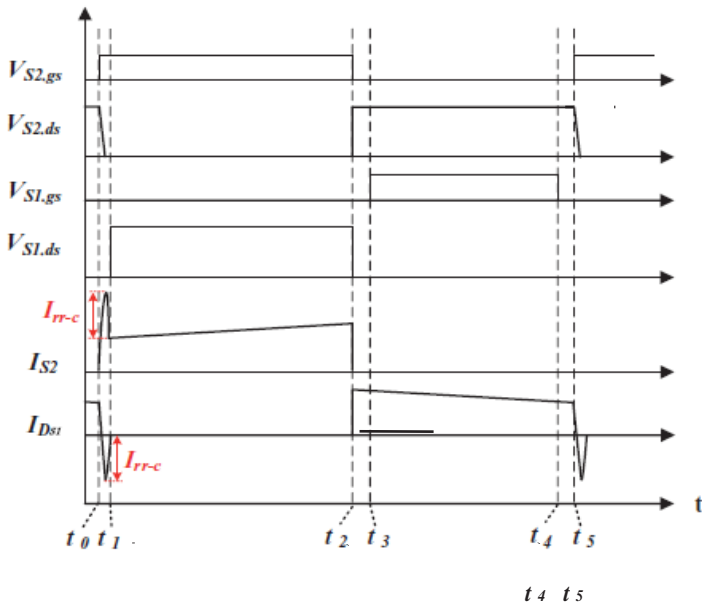


Fig. 4. Theoretical operating waveforms of the proposed bidirectional ac-dc rectifier in the rectification mode.

practical manner, it is significantly reduced as compared with the FRD operation.

At  $t_3$ , the gate signal  $V_{S1,gs}$  turns ON. Since the IGBTs cannot conduct in the reverse direction, the energy in the input voltage source and the inductor  $L_1$  is still discharged through SiC diode  $D_{S1}$ . In the rectification mode, the high-side SiC diodes instead of the IGBTs are fully operated during entire rectification modes. Therefore, the conduction loss of the high-side switches depends on the forward voltage drop of the SiC diodes. Other operation modes are not different from the conventional full-bridge rectifier using a unipolar switching method.

### B. Consideration for Switching Losses in a Generation Mode

In the generation mode using the same switching pattern as the rectification mode, the proposed bidirectional rectifier has five operating modes in a single switching cycle. The circuit operations in the positive half period of the input voltage are shown in Fig. 5. After the discharge operation of dc-link's energy, the antiparallel diode including the low-side switch  $S_2$  will be conducted by freewheeling operation using inductor's energy as shown in *Mode 2*. During this period, the energy stored in the output capacitance of  $S_2$  can be fully discharged. In *Mode 3*,  $S_2$  turns ON under the ZVS condition. Through these operation modes, the turn-on losses in the low-side switches can be reduced. When the high-side switch  $S_1$  turns ON in *Mode 5*, the antiparallel diode of  $S_2$  cannot immediately turn OFF because of poor reverse recovery performance of the MOSFET's antiparallel diode. It causes an additional switching loss on  $S_1$  through the reverse recovery current. Therefore, the generation mode using the same switching pattern of the rectification mode has advantages of soft switching and disadvantages of reverse recovery loss. The MOSFET's losses in the generation mode depend on the MOSFET's  $R_{DS,on}$  and the reverse recovery characteristics of the antiparallel diode. The selection of the MOSFET can determine the significant loss factor between

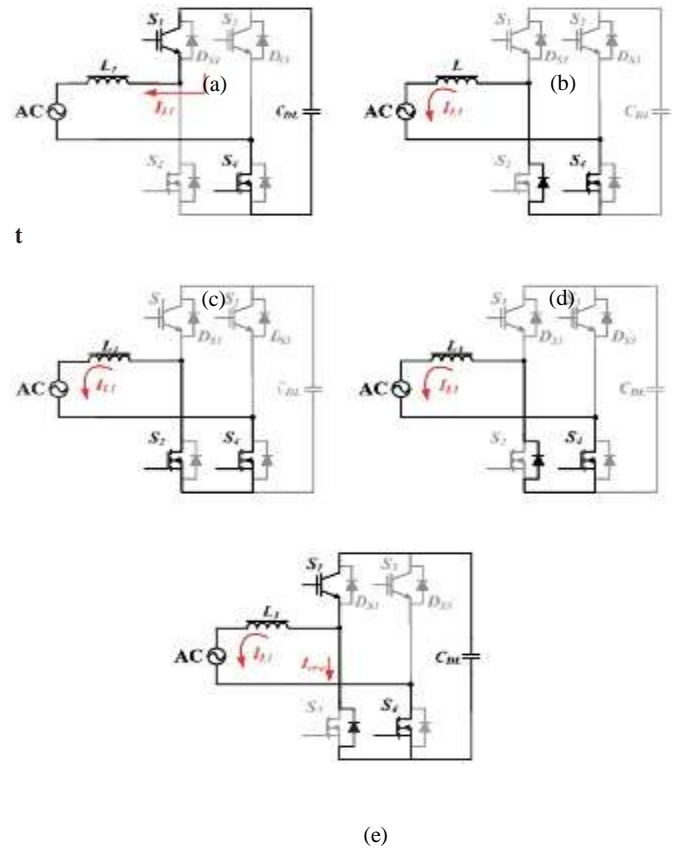


Fig. 5. Operating modes in the rectifier's generation mode using the same switching pattern as the rectification mode: (a) *Mode 1*, (b) *Mode 2*, (c) *Mode 3*, (d) *Mode 4*, and (e) *Mode 5*.

switching and conduction losses. However, if IGBTs are used for the low-side switches, the ZVS operation is not significant to reduce their switching loss. There are also reverse recovery losses through the reverse recovery characteristics of the antiparallel diode. They can increase the turn-off switching losses through the IGBT's tailing current.

If the reverse recovery loss through the MOSFETs is significant, it can be overcome employing the inverted switching pattern in the generation mode. The operation mode of the inverted switching pattern is shown in Fig. 6. In this operation, the switching pattern is perfectly inverted and the turn-on period of the high-side switches is one and half times longer than the turn-on period of the low-side switches. In *Mode 5*, the low-side switch  $S_4$  turns ON. At the same time, the reverse recovery current should be limited by the SiC diode  $D_{S3}$ . Using this switching pattern in the generation mode, there are no benefits of the ZVS operation. However, the reverse recovery losses can be significantly reduced as compared with the same switching pattern of the rectification mode. The modified switching pattern does not affect the power conversion and control performances of the ac-dc rectifier.

### C. Consideration for Conduction Losses

In the unipolar switching method, the turn-on period of low-side switches is one and half times longer than the turn-on

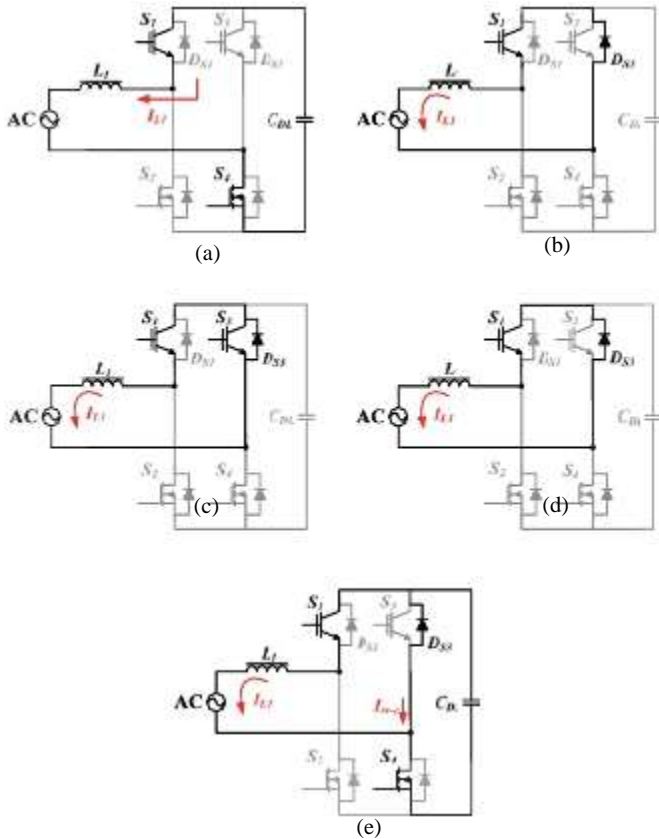


Fig. 6. Operating modes in the rectifier's generation mode using the inverted switching pattern against the rectification mode: (a) Mode 1, (b) Mode 2, (c) Mode 3, (d) Mode 4, and (e) Mode 5.

period of high-side switches. To analyze the conduction loss of MOSFETs as the low-side switches, the circuit operation of the proposed bidirectional rectifier assumes that inductor  $L_1$  is sufficiently large to operate CCM and the ac input current is a perfectly sinusoidal waveform. Generally, the conduction loss in MOSFETs can be calculated using the rms current passing through MOSFET's  $R_{DS,on}$ . Since the turn-on period of the low-side switches is 75% of the fundamental period of the ac input current, the rms current of the low-side switches can be calculated using the following equation:

where  $\eta$  is the power conversion efficiency.

Using the aforementioned equations, the total conduction losses of the rectifier's switches in the rectification can be

$$I_{\text{rms,low}} = \sqrt{\frac{1}{2\pi} \int_0^{\frac{3}{2}\pi} (I_{\text{in,P}} \sin \omega t)^2 d\omega t}$$

$$I_{\text{in,P}} = \sqrt{2} \frac{P_{\text{out}}}{\eta V_{\text{in,rms}}} \quad (2)$$

$$I_{\text{in,av}} = \frac{2}{\pi} I_{\text{in,P}} \quad (3)$$

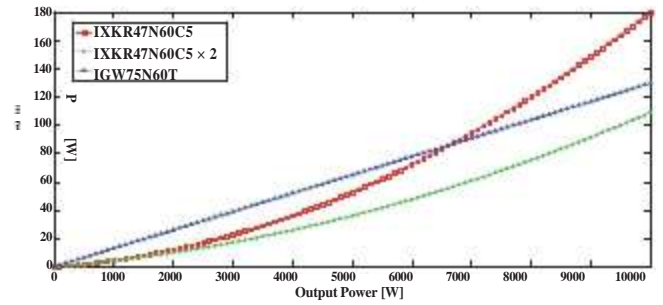


Fig. 7. Calculated conduction loss of rectifier switches in the rectification mode.

calculated as follows:

$$P_{\text{con-rec}} \approx 2(I_{\text{rms,low}})^2 R_{DS,on} + 2\left(\frac{1}{4} I_{\text{in,av}}\right) V_F$$

$$= \frac{3}{4} I_{\text{in,P}}^2 R_{DS,on} + \frac{1}{\pi} I_{\text{in,P}} V_F \quad (4)$$

where the conduction loss in the rectification mode is  $P_{\text{con-rec}}$  and  $V_F$  is the forward voltage drop of the high-side SiC diode, respectively. In comparison to using IGBTs for the low-side switches, Fig. 7 shows the calculated conduction losses using (4). The low-side switches use MOSFETs, which have extremely low  $R_{DS,on}$  (IXKR47N60C5) and the latest IGBTs (IKW75N60T), which have the very low collector-emitter threshold voltage  $V_{CE}$ . The high-side switches use SiC diodes (C3D20060D) as the antiparallel diode and IGBTs without antiparallel diode (IGW75N60T). The typical values of  $R_{DS,on}$ ,  $V_F$ , and  $V_{CE}$  are obtained from their datasheets. Since  $V_F$  and  $V_{CE}$  are almost the same value, the conduction loss in the generation mode is expected to be nearly the same as the conduction loss in the rectification mod,  $P_{\text{con-rec}}$ . In Fig. 7, the conduction losses of MOSFETs are less than the conduction losses of IGBTs under the load condition of 6.5 kW or less. Under the light-load condition, MOSFETs is better than IGBTs in the view point of the power conversion efficiency. At the rated load (5 kW), the difference of the conduction losses between MOSFETs and IGBTs is about 12 W. If two MOSFETs are used in parallel, the conduction losses in the rated load will be reduced about 30 W

#### . SRF-PLL With Enhanced Frequency Estimator

For the application of the grid-interactive power converter the phase estimation of the supply voltage is required to control the entire power system; especially, the phase information of the supply voltage is mandatory to generate the current reference. The phase estimation method requires robustness to noise and disturbance from grid, accuracy to the fundamental frequency variation and harmonic distortion, and easy implementation using analog or digital platforms. The SRF-PLL is one of the popular methods. It has a weak point of a frequency tracking performance. In Fig. 8, the constant angular frequency of the fundamental component  $\omega_s$  is used as a feedforward term for compensating the phase angle tracking. It can cause a tracking error in the PLL operation when the fundamental frequency

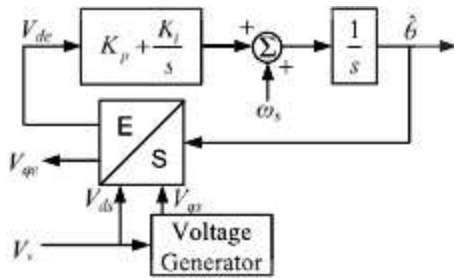


Fig. 8. Block diagram of a conventional single-phase SRF-PLL.

changes to the different value of the constant  $\omega_s$ . To track unexpected fundamental frequencies, the SRF-PLL requires a frequency estimator instead of the constant angular frequency.

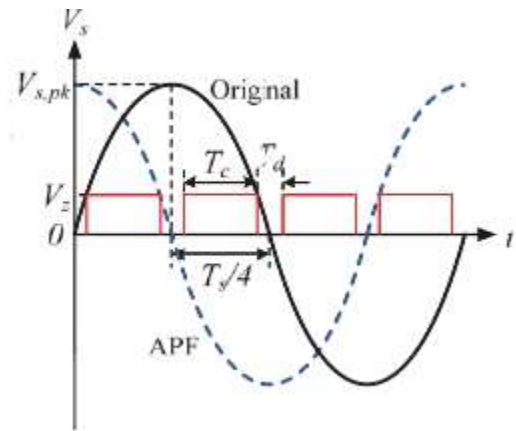
The SRF-PLL method uses the  $\pi/2$  phase-shifted wave of the supply voltage using the all-pass filter (APF). Therefore, the PLL has four zero crossing points in a period of the supply voltage and they are located at every  $\pi/2$ . It means that the frequency information can be obtained at every quarter of the period. However, the conventional research has updated the frequency information at every half of the period. Consequently, the proposed frequency detection algorithm illustrated in Fig. 9(a) can update the variation of the supply frequency two times faster than the conventional one. In the algorithm, there are two time zones to calculate the supply period:  $T_c$  and  $T_d$  where  $T_c$  is the time duration between two zero crossing points and  $T_d$  is the time duration near the zero crossing point.  $T_d$  is introduced to implement a practical PLL system using the proposed algorithm since noises in the power stage and sensors make the exact detection of the zero crossing points imperfect. In Fig. 9(a), the supply frequency can be estimated as shown in

$$\hat{f}_s = \frac{1}{4(T_c + T_d)}. \quad (5)$$

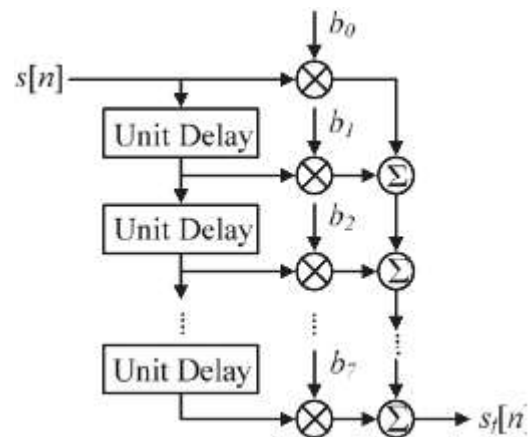
The FIR low-pass filter (LPF) illustrated in Fig. 9(b) is adopted to the proposed frequency detector instead of a moving average (MA). The filtered output can be calculated as follows:

$$s_f[n] = \sum_{k=0}^7 b_k s[n-k] \quad (6)$$

where  $s[n]$  is the  $n$ th input signal,  $s_f[n]$  is the  $n$ th filtered signal, and  $b_k$  is the  $k$ th-order filter coefficient. This filter has seventh order and uses the Blackman window to enhance the sharpness of the filter at the cut-off frequency and to suppress sidelobe components. It can improve the transient dynamics and reduce the steady-state error of the frequency detector. Fig. 9-(c) shows the block diagram of the single-phase SRF-PLL using the proposed frequency detector. The frequency detector calculates the fundamental frequency using (5) and it is added to the PI value of  $V_{dc}$  instead of the constant value to generate an accurate angle value with respect to frequency variations. In addition, the calculated frequency is used in the voltage generator which makes the orthogonal waveform to the supply voltage.



(a)



(b)

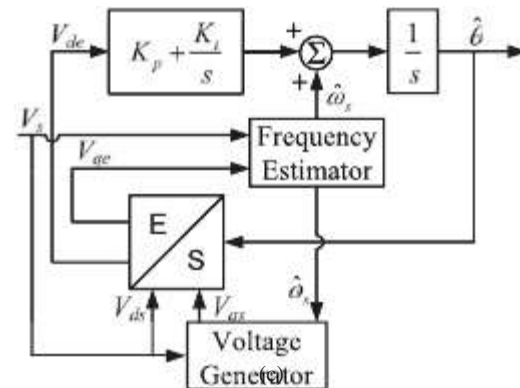


Fig. 9. Proposed single-phase PLL method: (a) frequency detection algorithm using zero crossing and APF, (b) block diagram of the seventh-order FIR filter, and (c) block diagram of the PLL using the proposed frequency estimator.

Fig. 10 shows the comparison of the frequency detection speeds of three methods: half-cycle detection (HD) with MA quad-cycle detection (QD) with MA, and QD with FIR filter using the Psim simulation software. The simulation result of the HD with MA, which is the conventional one, shows high fluctuation and long settling time in the fundamental frequency detection. However, the simulation result of QD with MA shows low fluctuation and short settling time because of the shorter update duration than the case of HD. In addition, QD with FIR



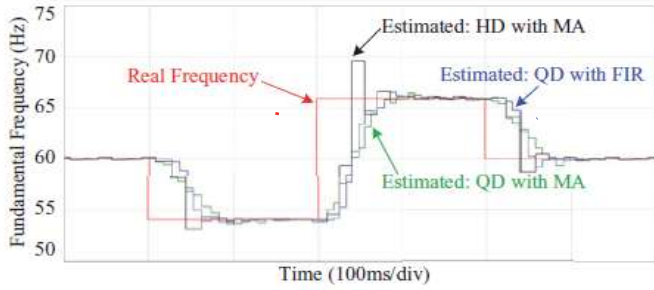


Fig. 10. Simulation results of the proposed single-phase PLL for comparison of frequency detection speed.

filter has higher transient dynamics and faster convergence than the case of QD with MA because of the seventh-order FIR filter using the Blackman window instead of MA.

#### IV. ISOLATED BIDIRECTIONAL CLLC RESONANT CONVERTER

In this section, the design methodology of the power stages of the proposed bidirectional CLLC resonant converter will be discussed. The new control schemes are proposed to decide power flow directions and to regulate output voltage under bidirectional power flows. In addition, the dead-band control algorithm is proposed to smoothly change the power conversion direction only using output voltage information. This algorithm is based on a hysteresis control method to decide the power flow direction of bidirectional converters.

##### A. Gain Analysis Using the FHA model

The first harmonic approximation (FHA) model and operation mode in the proposed CLLC resonant converter are already introduced in [18]. Fig. 11 shows the equivalent circuit of the proposed full-bridge bidirectional CLLC resonant converter using the FHA method. The resonant network of the converter is composed of the series resonant capacitor  $C_r = C_{r1} = C_{r2}$ , the equivalent series resonant inductance  $L_{eq}$ , and the magnetizing inductance  $L_m$ . Since the turn ratio of the transformer is 1:1, it does not affect the circuit model and  $L_{eq}$  equals the twice of the series resonant inductance  $L_r = L_{r1} = L_{r2}$ . The forward transfer function  $H_r$  of the resonant network can be derived as shown in

$$H_r(s) = \frac{V_{o,FHA}(s)}{V_{i,FHA}(s)} = \frac{Z_o(s)}{Z_{in}(s)} \cdot \frac{R_{o,\epsilon}}{(sC_r)^{-1} + R_{o,\epsilon}} \quad (7)$$

$$Z_{in}(s) = \frac{1}{sC_r} + sL_{eq}(s) + Z_o(s) \quad (8)$$

$$L_{eq}(s) = \frac{L_r}{s^2 L_m L_r [R_o(sL_m + sL_r + R_o)]^{-1} + 1} \quad (9)$$

$$Z_o(s) = \frac{L_m C_r^{-1} + sL_m R_{o,\epsilon}}{sL_m + (sC_r)^{-1} + R_{o,\epsilon}}, R_{o,\epsilon} = \frac{8}{\pi^2} R_o \quad (10)$$

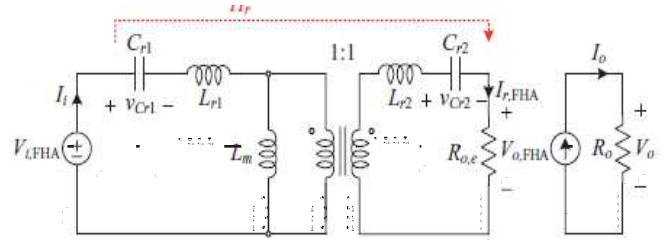


Fig. 11. FHA model of the proposed bidirectional CLLC resonant converter.

Therefore, the gain of converter  $\|H_r\|$  can be derived as follows:

$$\frac{V_o}{V_{in}} = \|H_r(f_n)\| = \frac{f_n^3}{\sqrt{f_n^2 A^2(f_n) + Q^2 B^2(f_n)}} \quad (11)$$

where  $A(f_n)$  and  $B(f_n)$  are the function components as follows:

$$A(f_n) = -f_n^2(1+k) + k \quad (12)$$

$$B(f_n) = f_n^4 - f_n^2(2+k) + k. \quad (13)$$

In addition,  $f_n$  can be described using the resonant frequency  $f_r$ ,  $Q$  is the quality factor, and  $k$  is the inductance ratio between the magnetizing and leakage inductance, respectively, given by

$$f_n = \frac{f_s}{f_r}, f_r = \frac{1}{2\pi\sqrt{L_r C_r}}, Q = \frac{Z_r}{R_{o,\epsilon}}, Z_r = \sqrt{\frac{L_r}{C_r}}, k = \frac{L_r}{L_m} \quad (14)$$

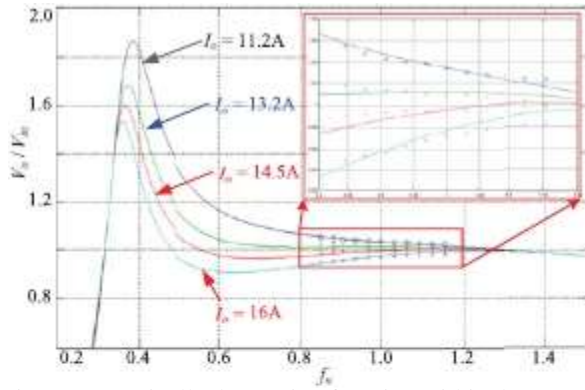
Fig. 12 (a) shows the gain curve according to load current and normalized frequency at  $L_m = 130 \mu\text{H}$ . The gain has a peak value at low resonant frequency which contains the magnetizing inductance as a resonant component. At high resonant frequency, the gain of the converter is slightly higher than unity gain. Under the light-load condition, the gain is high and the slope of the gain curve is sharp. However, the overall value of the gain curve is decreasing under the heavy-load condition. The higher load induces the lower gain in the proposed bidirectional CLLC resonant converter.

##### B. Soft-Switching Conditions

The ZVS operation of the primary power MOSFETs and the soft commutation of the output rectifiers are significant factors for the efficiency-optimal design of the bidirectional full-bridge CLLC resonant converter. The lower operating frequency than the resonant frequency can guarantee the soft commutation of the output rectifiers because the difference between the switching frequency and the resonant frequency makes discontinuous rectifying current. In addition, during the dead time of the switches, the primary current should discharge the output capacitance of four primary switches for their ZVS turn-on. Therefore, the magnetizing inductance is limited by the maximum operating frequency as shown in

$$f_s \leq f_r \quad (15)$$

$$L_m \leq \frac{t_{dt}}{16C_S f_{s,\max}} = \frac{t_{dt}}{16C_S f_r} \quad (16)$$



gain is a monotonically decreasing function within the operating (a)

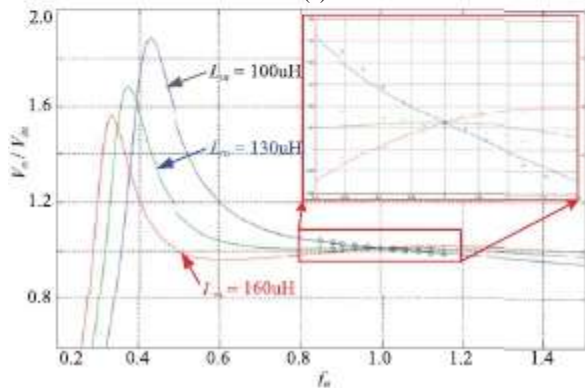


Fig. 12. Theoretical gain curves according to normalized frequency. (a) According to load current ( $L_m = 130 \mu\text{H}$ ). (b) According to magnetizing inductance at full load (5 kW).

Inequality (16) shows that small  $L_m$  can guarantee the ZVS of main switches. However, small  $L_m$  also increases the conduction loss of MOSFETs, transformer windings, and output rectifiers in the primary and secondary sides. On the other hand, the large magnetizing inductance satisfied with (16) can reduce the conduction loss and improve the power conversion efficiency of the converter. However, large  $L_m$  can make a gain reduction below the unity gain in the proposed bidirectional CLLC resonant converter. Fig. 12(b) shows the gain curve according to the magnetizing inductance and normalized frequency. At higher magnetizing inductance than  $160 \mu\text{H}$ , the gain curve does not monotonically decrease. Under this condition, when the load increases or the input voltage decreases, the conventional PI controller cannot regulate the output voltage.

### C. Design Guide for a Limited Gain Curve

In order to obtain the monotonic gain curve according to the operating frequency, the resonant components of  $L_m$ ,  $L_r$ , and  $C_r$  should be selected considering proper  $f_r$  for the operating frequency, and proper  $Q$  and  $k$  for the available gain curve higher than the unity gain. The resonant network in the proposed bidirectional CLLC resonant converter should be designed to keep the gain of the converter higher than the unity gain with respect to entire load range. The monotonic gain curve can regulate the output voltage employing a linear feedback controller. Using the polarity of the gain function's derivative with respect to  $f_n$  the gain can be decided to whether a monotonically decreases

$$\frac{d}{df_n} \|H_r(f_n)\| = \frac{2kf_n^4 A(f_n) - Q^2 f_n^2 B(f_n) C(f_n)}{[f_n^2 A^2(f_n) + Q^2 B^2(f_n)]^{1.5}} \quad (17)$$

function or not. The derivative of (11) can be derived follows: where  $C(f_n)$  is the function component as shown in

$$C(f_n) = f_n^4 + f_n^2(2 + k) - 3k. \quad (18)$$

he derivative of the gain curve has to be negative if the

frequency. The polarity of (17) is decided by only the value of its numerator because the denominator of (17) is always positive. For the quality factor  $Q$ , an inequality can be derived using the numerator of (17) as shown in

$$Q < \sqrt{\frac{2kf_{n,\max}^2 A(f_{n,\max})}{B(f_{n,\max})C(f_{n,\max})}}, 0 < k < 1. \quad (19)$$

$$I_o < \frac{8V_o Q}{\pi^2 Z_r}. \quad (20)$$

### D. Dead-Band Control for Bidirectional Operation

Fig. 13(a) shows the theoretical waveforms of the proposed dead-band control algorithm for the bidirectional CLLC resonant converter. When the load becomes negative, the output voltage of the converter will drastically increase because power is supplied to the output capacitor from two sides: the converter side and the load side. At this time, the converter is uncontrollable without changing the power conversion mode because of the negative power flow. If the output voltage reaches the positive dead-band voltage  $+V_{\text{band}}$ , the power conversion mode changes from the powering mode to the generating mode. In this generating mode, the converter transfers power from load to input side. Then, the output voltage will decrease to the reference voltage  $V_{\text{ref}}$ , which will be regulated by a pulse frequency modulation (PFM) controller. In the same manner, the power conversion mode can be changed from the generating mode to the powering mode. When the load becomes positive, the output voltage will decrease to the negative dead-band voltage  $-V_{\text{band}}$ . Then, the power conversion mode is changed and the output voltage will increase to  $V_{\text{ref}}$ .

Fig. 13(b) shows the block diagram of the proposed digital controller. The dead-band controller can select the power conversion mode using the voltage gap  $V_{\text{gap}}$  which is the voltage difference between the output voltage and the dead-band voltage. This dead-band controller generates the sign of the voltage error  $V_{\text{err}}$  which is the voltage difference between the output voltage and the reference voltage. The PI controller regulates the output voltage using  $V_{\text{err}}$  and its sign. The switch control block generates PFM switching pulses using the calculated



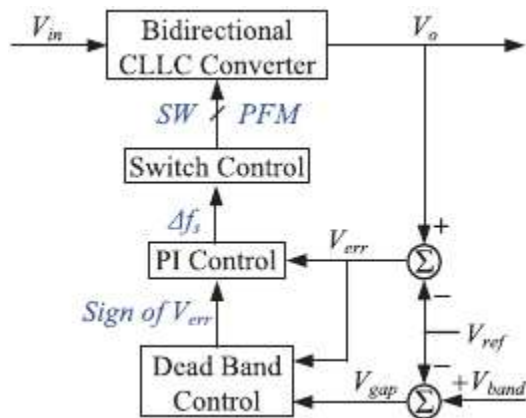
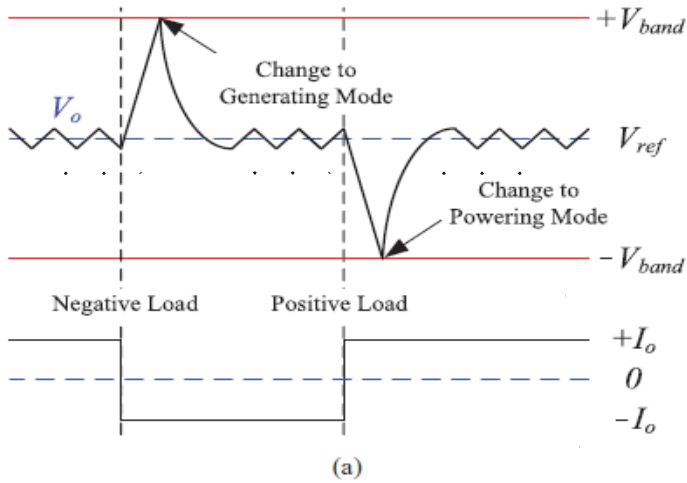


Fig. 13. Schematics of the proposed dead-band control algorithm: (a) theoretical waveforms and (b) block diagram of the control algorithm.

switching frequency generated by the PI controller. Finally, the PFM switching pulses are assigned to the proper power switches considering the power conversion mode.

## V. EXPERIMENTAL RESULTS

Table I shows the designed parameters of the proposed prototype converter. A 5-kW isolated bidirectional ac–dc converter has been designed and evaluated at 220 Vac input voltage. This prototype converter used a DSP of TI's TMS320F28335 as a digital controller to implement the proposed control algorithms: the unipolar SPWM control for the bidirectional ac–dc rectifier, the proposed SRF-PLL algorithm, the PFM control for the bidirectional CLLC resonant converter, and the dead-band and switch transition controls for the bidirectional power conversion. The switching frequency of the ac–dc rectifier is 13.8 kHz and the dc–dc converter operates within the range of 58–65 kHz. The magnetizing inductance is selected as 130  $\mu\text{H}$  in the prototype dc–dc converter which is the overload condition containing 10% margin from the rated load of 5 kW. Fig. 14 shows the configuration of the prototype converter.

As shown in Fig. 15(a), the line voltage and current waveforms of the bidirectional ac–dc rectifier under the 5-kW full-load condition are almost in phase. From this result, the

TABLE I  
DESIGN SPECIFICATIONS OF THE PROTOTYPE ISOLATED BIDIRECTIONAL AC–DC CONVERTER

Specifications	Values
Input voltage ( $V_{in}$ )	AC 220 V
Output Voltage ( $V_{out}$ )	DC 380 V
Rated Power ( $P_{out}$ )	5 kW
$S_1$ and $S_3$	IGW75N60T
$D_{S1}$ and $D_{S2}$	C3D20060D
$S_2$ and $S_4$	IXKR47N60C5
$Q_1 \sim Q_8$	SPW47N60CFD
$T_r$	EE6565(PM7)
$L_1$	1.6 mH
$L_m$	130 $\mu\text{H}$
$L_r$	30 $\mu\text{H}$
$C_r$	200 nF

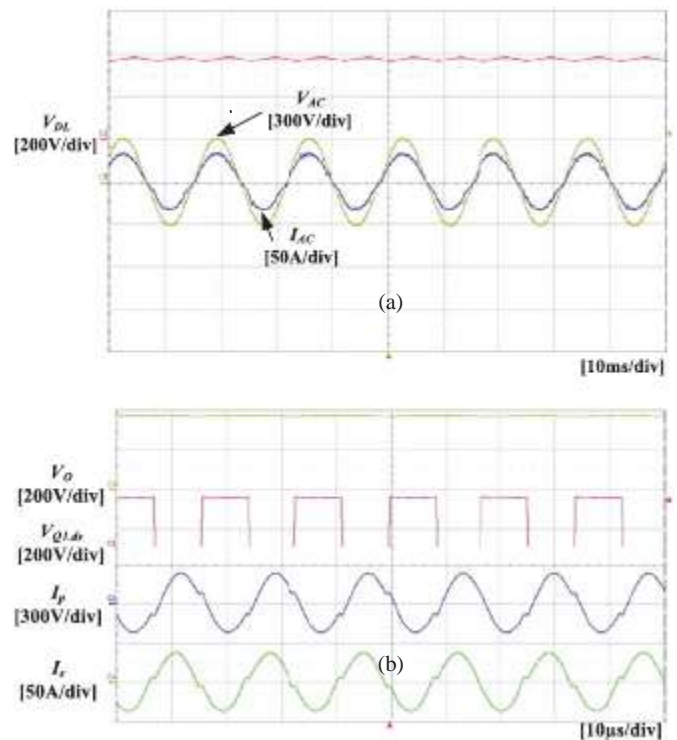
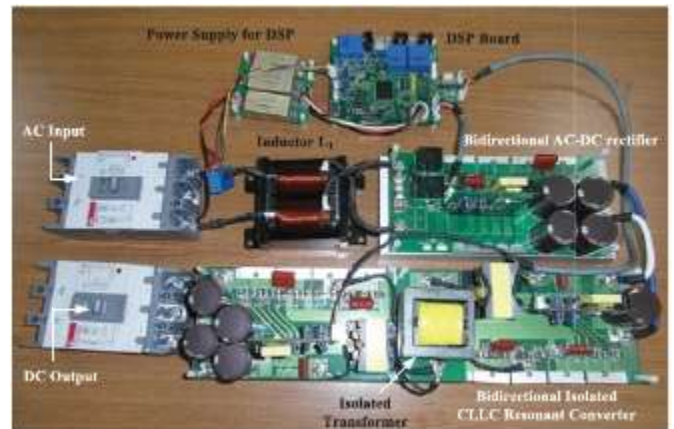


Fig. 15. Experimental waveforms at full load (5 kW): (a) input voltage and current with dc-link voltage in the ac–dc rectifier and (b) resonant currents with output voltage in the dc–dc converter.

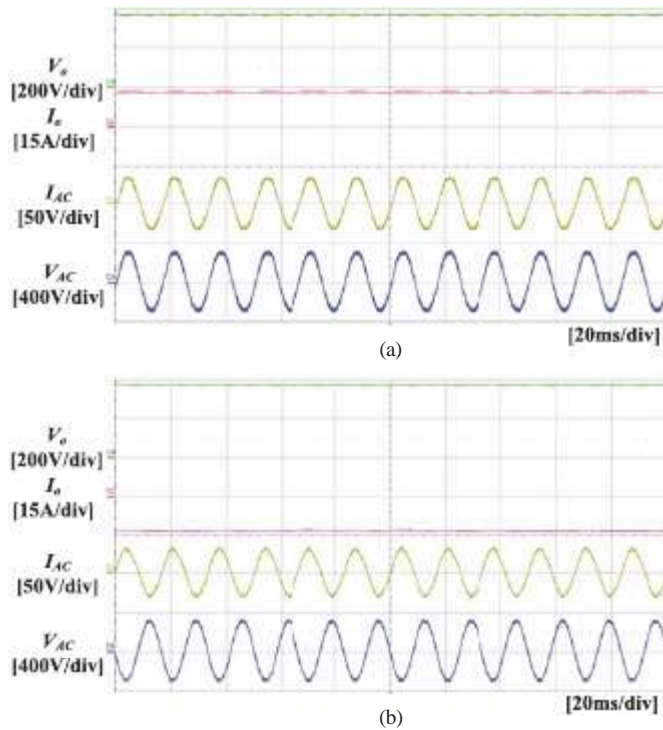


Fig. 16. Experimental waveforms of the bidirectional operation at full load: (a) rectification mode and (b) generation mode.

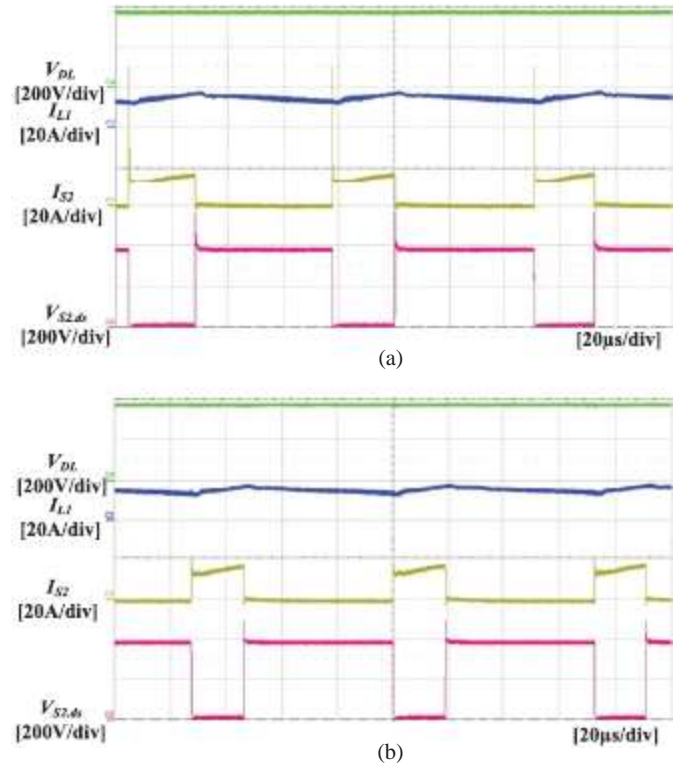


Fig. 17. Switching waveforms of the ac-dc rectifier using FRD and SiC diode: (a) FRD case and (b) SiC diode case.

proposed SRF-PLL is well operated under the steady-state condition. Fig. 15(b) shows experimental waveforms of the proposed bidirectional *CLLC* resonant converter at the full load. The figure illustrates the waveforms of the drain-source voltage of  $Q_1$ , the primary current and the secondary current, and the output voltage. At the full load, the operating frequency of the converter is 58 kHz and the primary current and the secondary current are almost sinusoidal because of the converter's operation near the resonant frequency determined by the designed resonant network. All the waveforms are measured in the powering mode; however, the generating mode has the same waveforms because of the converter's symmetric structure. The current waveforms show that the ZVS of the primary switches and the soft commutation of the secondary rectifiers are well achieved under the full-load condition.

The experimental measurement data of the proposed gain analysis method are shown in Fig. 12(a) and (b). The gains of the converter were measured with respect to specific operating frequencies. Errors between simulation expectations and experimental measurements were made due to the imperfection of the FHA modeling. However, the tendency of the gain characteristics can be expected using the FHA methods.

The measured waveforms of the ac input voltage and current at positive and negative full-load conditions (5 and -5 kW) are shown in Fig. 16(a) and (b), respectively. Fig. 16(a) shows that the prototype ac-dc rectifier operates in the rectification mode with the grid synchronization operation to convert ac-grid power to dc bus under the full-load condition. Fig. 16(b) shows the generation mode to send surplus power from the dc bus to the ac grid. From these results, the bidirectional operation of the

prototype rectifier in both the rectification mode and the generation mode is verified. Fig. 17(a) and (b) shows the switching waveforms of the ac-dc rectifier using FRD and SiC diode, respectively. In Fig. 17(a), there are high current spike of  $I_{S2}$  and high voltage spike of  $V_{S2,ds}$  because of high reverse recovery current from the FRD diode when it turns OFF. However, the current and voltage spikes are reduced in Fig. 17(b) since the SiC diode which has very small reverse recovery charge replaces the FRD diode. The low reverse recovery current can increase the power conversion efficiency of the ac-dc rectifier and reduce heat emission from rectifying diodes and switching MOSFETs in the rectifier.

Fig. 18(a) shows the experiment results of phase detection performance using the conventional SRF-PLL under the fundamental frequency fluctuation from -10% to +10%. It has tracking errors while the fundamental frequency changes to the different value from the constant angular frequency. Fig. 18(b) shows the experimental results of the phase detection performance using the proposed SRF-PLL method. The phase detector of the proposed PLL can follow the step-changed phase angle within two fundamental periods. It verifies that the proposed PLL has good performance of the phase angle tracking.

Fig. 19(a) and (b) shows the experimental waveform of the step load response of the prototype dc-dc converter in the case of the bidirectional power conversion, respectively. In Fig. 19(a), the distortion level of the output voltage is around 10 V during the mode transition of the power conversion way because the dead-band voltage  $V_{band}$  is set to 10 V in the prototype controller at the step load changes from 2.5 to -2.5 kW and vice versa. In



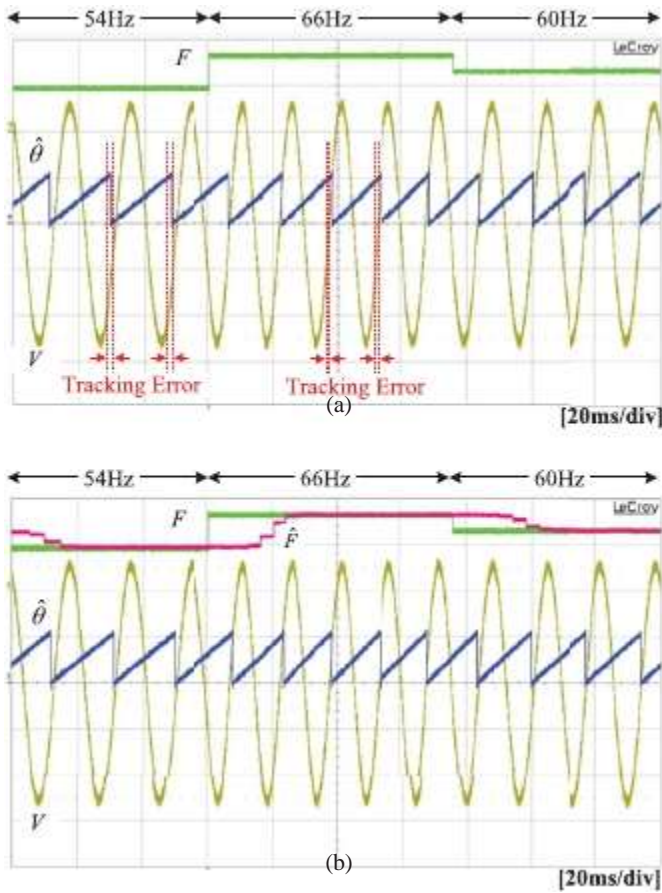


Fig. 18. Experimental results of phase detection performance: (a) conventional SRF-PLL and (b) proposed PLL.

Fig. 19(b), when a bidirectional step load changes from 2.5 to -2.5 kW, the ac input current smoothly changed its phase angle within two cycles using the proposed SRF-PLL. Fig. 19 verifies that the proposed dead-band controller and SRF-PLL are well designed to change the power flow direction smoothly.

Fig. 20 shows efficiency curves of the prototype ac-dc rectifier, dc-dc converter, and overall converter system, respectively. They are measured at the input voltage of 220 Vac. Fig. 20(a) shows the power conversion efficiency in the rectification mode. The maximum efficiency of rectifier is 98.6% at 2 kW. In addition, the bidirectional CLLC resonant converter has a good efficiency characteristic under middle- and high-load conditions. The power conversion efficiency is higher than 97.5% at more than 50% (2.5 kW) of the full load. Finally, the power conversion efficiency of the overall converter system is 94.5% at the rated output power of 5 kW. The maximum efficiency is almost 96% at 2.5 kW. Fig. 20(b) shows the power conversion efficiency in the generation mode. The maximum efficiency of the rectifier is 98.3%. The efficiency of the bidirectional CLLC resonant converter is the same as the efficiency of the rectification mode because of its symmetric structure. The power conversion efficiency of the overall converter system is 94.2% at 5 kW and at 95.6% at 2.5 kW.

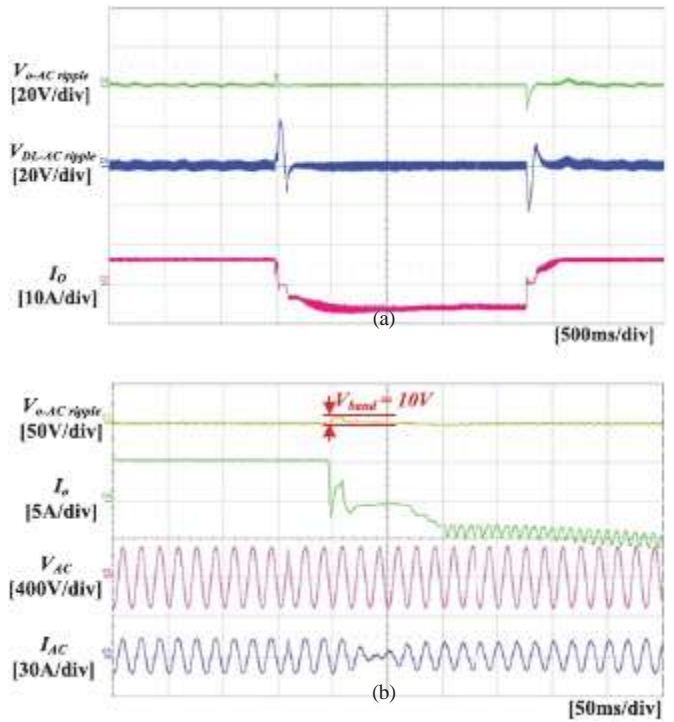


Fig. 19. Step load response (bidirectional power conversion from 2.5 to -2.5 kW) of overall bidirectional converter: (a) dc-dc converter part and (b) ac-dc rectifier part.

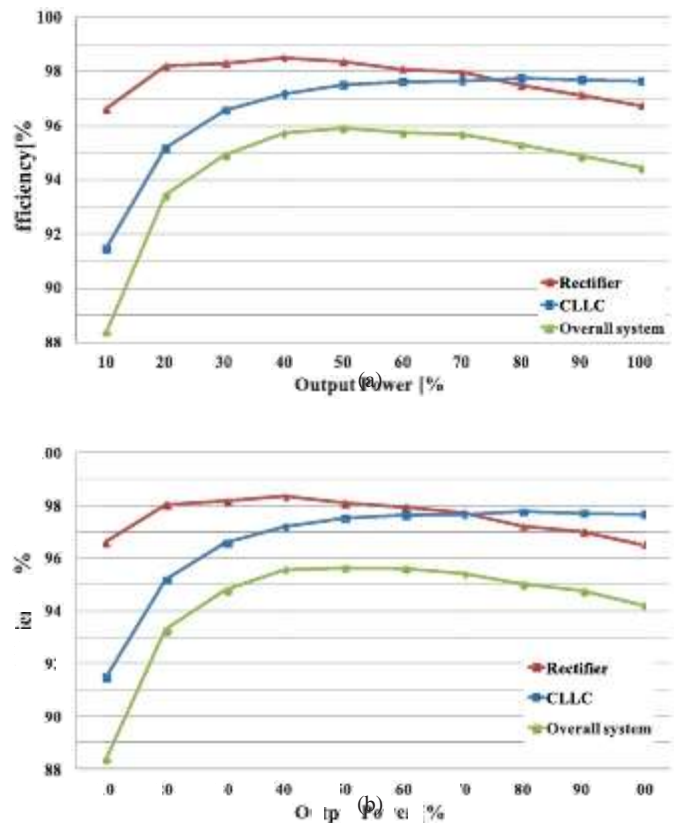


Fig. 20. Power conversion efficiency curves of the ac-dc rectifier, dc-dc converter, and overall converter system: (a) rectification mode and (b) generation mode.



## VI. CONCLUSION

The isolated bidirectional ac–dc converter is proposed for the 380-V dc power distribution system to control the bidirectional power flow and to improve its power conversion efficiency. In order to improve the reverse recovery problem, the high-side switches of the ac–dc rectifier employ IGBTs without antiparallel diodes and SiC diodes. In addition, the low-side switches are composed of two MOSFETs to reduce the conduction loss in the rectification mode. For comparison with the conventional IGBT switches, the total conduction losses of the rectifier's switches are calculated in the rectification mode. The simple and intuitive frequency detection method for the single-phase SRF-PLL is also proposed using the filter compensator, fast QD, and FIR filter to improve the robustness and accuracy of the PLL performance under fundamental frequency variations. The proposed PLL system shows lower detection fluctuation and faster transient response than the conventional techniques. Finally, the proposed *CLLC* resonant converter can operate under the ZVS for the primary switches and the soft commutation for the output rectifiers. The soft-switching condition of the converter is derived to obtain the design methodology of the resonant network. Gain properties are also analyzed to avoid gain reduction and nonmonotonic gain curve under high-load conditions. In addition, the dead-band and switch transition control algorithms are proposed to smoothly change the power flow direction in the converter. From light to full load, the overall power conversion efficiency of the 5-kW prototype converter was measured to almost 96% at 2.5 kW and 94.5% at the full load of 5 kW.

## REFERENCES

- [1] G.-S. Seo, J. Baek, K. Choi, H. Bae, and B. Cho, "Modeling and analysis of dc distribution systems," in *Proc. IEEE 8th Int. Conf. Power Electron. ECCE Asia*, May 2011, pp. 223–227.
- [2] K. Techakittiroj and V. Wongpaibool, "Co-existence between ac-distribution and dc-distribution: In the view of appliances," in *Proc. 2nd Int. Conf. Comput. Electrical Eng.*, Dec. 2009, vol. 1, pp. 421–425.
- [3] A. Stupar, T. Friedli, J. Miniobock, and J. Kolar, "Towards a 99% efficient three-phase buck-type PFC rectifier for 400-V dc distribution systems," *IEEE Trans. Power Electron.*, vol. 27, no. 4, pp. 1732–1744, Apr. 2012.
- [4] T.-F. Wu, C.-L. Kuo, K.-H. Sun, and Y.-C. Chang, "DC-bus voltage regulation and power compensation with bi-directional inverter in dc-microgrid applications," in *Proc. IEEE Energy Convers. Congr. Expo.*, Sep. 2011, pp. 4161–4168.
- [5] B.-R. Lin and Z.-L. Hung, "A single-phase bidirectional rectifier with power factor correction," in *Proc. IEEE Energy Convers. Congr. Expo.*, Aug. 2001, vol. 2, pp. 601–605.
- [6] Y. Zhangang, C. Yanbo, and W. Chengshan, "Construction, operation and control of a laboratory-scale microgrid," in *Proc. Int. Conf. Sustainable Power Generation Supply*, Apr. 2009, pp. 1–5.
- [7] W. Ryckaert, K. De Gussemé, D. Van de Sype, L. Vandeveldé, and J. Melkebeek, "Damping potential of single-phase bidirectional rectifiers with resistive harmonic behaviour," *IEE Electric Power Appl.*, vol. 153, no. 1, pp. 68–74, Jan. 2006.
- [8] T.-F. Wu, K.-H. Sun, C.-L. Kuo, and C.-H. Chang, "Predictive current controlled 5-kW single-phase bidirectional inverter with wide inductance variation for dc-microgrid applications," *IEEE Trans. Power Electron.*, vol. 25, no. 12, pp. 3076–3084, Dec. 2010.
- [9] D. Dong, F. Luo, D. Boroyevich, and P. Mattavelli, "Leakage current reduction in a single-phase bidirectional ac-dc full-bridge inverter," *IEEE Trans. Power Electron.*, vol. 27, no. 10, pp. 4281–4291, Oct. 2012.
- [10] K. H. Edelmöser and F. A. Himmelstoss, "Bidirectional dc-to-dc converter for solar battery backup applications," in *Proc. IEEE 35th Annu. Power Electron. Spec. Conf.*, Jun. 2004, vol. 3, pp. 2070–2074.

- [11] D. Salomonsson, L. Söder, and A. Sannino, "Protection of low-voltage dc microgrids," *IEEE Trans. Power Del.*, vol. 24, no. 3, pp. 1045–1053, July 2009.
- [12] J. Rekola and H. Tuusa, "Comparison of line and load converter topologies in a bipolar LVDC distribution," in *Proc. 14th Eur. Conf. Power Electron. Appl.*, Aug./Sep. 2011, pp. 1–10.
- [13] B. Zhao, Q. Yu, and W. Sun, "Extended-phase-shift control of isolated bidirectional dc-dc converter for power distribution in microgrid," *IEEE Trans. Power Electron.*, vol. 27, no. 11, pp. 4667–4680, Nov. 2012.
- [14] R. Mirzahosseini and F. Tahami, "A phase-shift three-phase bidirectional series resonant dc/dc converter," in *Proc. 37th Annu. Conf. IEEE Electron. Soc.*, Nov. 2011, pp. 1137–1143.
- [15] W. Li, H. Wu, H. Yu, and X. He, "Isolated winding-coupled bidirectional ZVS converter with PWM plus phase-shift (PPS) control strategy," *IEEE Trans. Power Electron.*, vol. 26, no. 12, pp. 3560–3570, Dec. 2011.
- [16] K. Wu, C. de Silva, and W. Dunford, "Stability analysis of isolated bidirectional dual active full-bridge dc-dc converter with triple phase-shift control," *IEEE Trans. Power Electron.*, vol. 27, no. 4, pp. 2007–2017, Apr. 2012.
- [17] W. Chen, P. Rong, and Z. Lu, "Snubberless bidirectional dc-dc converter with new CLLC resonant tank featuring minimized switching loss," *IEEE Trans. Ind. Electron.*, vol. 57, no. 9, pp. 3075–3086, Sep. 2010.

AUTHORS

**B. KRISHNAKANTH** received his B.Tech degree in Electrical and Electronics Engineering from SKR College of Engineering and Technology, Kondurusatram, Nellore dist, affiliated to JNTU Ananthapur. He is currently pursuing M.Tech power electronics in Brahmaiah college of engineering, north rajupalem, SPSR Nellore (Dist), affiliated to JNTU Ananthapur,



**P. SIVA KRISHNA** received his B.Tech Degree in Electrical and Electronics Engineering from Narayana engineering college, Nellore affiliated to jntu ananthapur. He received his M.Tech from sree venkataperumalu engineering college puttur, chitter dist. He has 1 years teaching experience, presently working as Professor of EEE, Brahmaiah college of engineering Affiliated to JNTU, Anantpur. Andhra Pradesh, India.

